Chemical Science

EDGE ARTICLE

View Article Online
View Journal | View Issue

Cite this: *Chem. Sci.*, 2023, **14**, 8321

Received 24th May 2023
Accepted 30th May 2023

DOI: 10.1039/d3sc02622a

rsc.li/chemical-science

Feasible bottom-up development of conjugated microporous polymers (CMPs) for boosting the deep removal of sulfur dioxide†

He Li,[a] Hanqian Pan,[b] Yijian Li,[b] Shuaishuai Shang,[a] Shihui Huang,[a] Xili Cui, *[b] Jun Hu *[a] and Honglai Liu[a]

A pain-point for material development is that computer-screened structures are usually difficult to realize in experiments. Herein, considering that linkages are crucial for building functional nanoporous polymers with diverse functionalities, we develop an efficient approach for constructing target-specific conjugated microporous polymers (CMPs) based on screening feasible polymerization pathways. Taking the deep removal of SO_2 from a SO_2/CO_2 mixture as the specific target, we precisely screen the linkages and fabricate different CMPs by manipulating the porosity and hydrophobicity. Based on the optimized Buchwald–Hartwig amination, the obtained CMPs can achieve SO_2/CO_2 selectivity as high as 113 and a moderate Q_{st} of 30 kJ mol^{-1} for feasible regeneration. Furthermore, the potential of CMPs for practical SO_2/CO_2 separation is demonstrated through continued breakthrough tests. The SO_2 binding sites are consistent with the screening results and proved by *in situ* Fourier transform infrared spectroscopy and grand canonical Monte Carlo simulation, providing solid feasibility for synthesis realizability for future boosts of task-specific CMPs.

Introduction

Deep removal of SO_2 is of great significance because of its serious environmental hazards.[1,2] Especially when addressing the challenge of carbon neutrality, the presence of SO_2 in flue gas is detrimental to CO_2 capture and utilization (CCU) since acidic SO_2 will preferentially bind with amine-based absorption solvents or adsorbents; meanwhile, even residual SO_2 may cause the deactivation of metallic catalysts for CO_2 chemical conversion.[3–6] Compared with conventional wet and dry flue gas desulfurization processes such as alkaline slurry scrubbing and lime spray drying, reversible physical adsorption *via* porous materials such as zeolites and activated carbon is recognized as a sustainable energy-saving technology for SO_2 removal.[7–10] However, SO_2 and CO_2 are both acidic gases and have similar kinetic sizes (0.4 nm for SO_2 *vs.* 0.33 nm for CO_2), making the selective adsorption of SO_2 over CO_2 full of challenges.

Recent years have witnessed a surge in metal–organic frameworks (MOFs) with good SO_2/CO_2 separation performance.[11–14] In these state-of-the-art MOFs, creating open metal sites,[15–17] introducing strong host–guest interaction,[18–20] as well as the gate-opening effect in MOFs[21] have been applied to enhance the deep desulfurization performance. Nevertheless, most MOFs are unable to withstand strong corrosive SO_2 or moisture, which usually results in irreversible structural collapse.[15,19,22] Therefore, the stable skeleton becomes one of the most critical factors for long-term SO_2 removal service during the design of porous materials. Alternatively, conjugated microporous polymers (CMPs) that are constructed using pure organic elements would exhibit promising characteristics of high acid tolerance and water resistance. Moreover, the combination of intrinsic microporous structures and designable task-specific binding sites would endow them with great potential for the efficient removal of SO_2.[23]

Although thousands of CMPs have been developed, the one committing to deep desulfurization has been rarely reported. Considering that computer-screened structures of CMPs from billions of possible monomers may be invalid in realistic synthesis and trial-and-error experimental approaches are extremely chemically expensive and time-consuming,[24] the efficient bottom-up development of CMPs for boosting the deep removal of SO_2 is still full of challenges. From a realistic synthesis perspective, feasible coupling reactions for the CMPs' construction are limited, and if we screen from linkages extracted from the limited coupling reactions, rather than randomly from billions of monomers, the synthesis realizability of the screened CMPs can be guaranteed. Moreover, as each linkage corresponding to one specific coupling reaction can be formed by diverse monomers, we can further regulate the

[a]State Key Laboratory of Chemical Engineering, School of Chemistry and Molecular Engineering, East China University of Science and Technology, 130 Meilong Road, Shanghai, 200237, China. E-mail: junhu@ecust.edu.cn

[b]Key Laboratory of Biomass Chemical Engineering of Ministry of Education, College of Chemical and Biological Engineering, Zhejiang University, Hangzhou, 310027, China. E-mail: cuixl@zju.edu.cn

† Electronic supplementary information (ESI) available. See DOI: https://doi.org/10.1039/d3sc02622a

functionality and porous structure, simultaneously, to achieve task-specific applications.

Results and discussion

To this end, there are six typical coupling reactions for CMPs' construction that are Suzuki–Miyaura cross-coupling, Heck reaction, Sonogashira–Hagihara cross-coupling, Buchwald–Hartwig amination, cyclotrimerization, and thioether connection, resulting in the linkages of carbon–carbon single bonds (–C–C–), carbon–carbon double bonds (–C=C–), carbon–carbon triple bonds (–C≡C–), secondary amine (–NH–), triazine (–C_3N_3–), and thioether (–S–), respectively. As shown in Fig. 1, the SO_2 binding energies (BEs) of different linkages are in the order of –NH– (21.42 kJ mol^{-1}) > –C≡C– (14.88 kJ mol^{-1}) > –C_3N_3– (13.82 kJ mol^{-1}) > –C–C– (11.76 kJ mol^{-1}) > –C=C– (11.52 kJ mol^{-1}) > –S– (7.4 kJ mol^{-1}). In comparison, the BEs of CO_2 are much lower in the range of 5.78–7.92 kJ mol^{-1} due to its lower polarity (Fig. S1–S4†). Consequently, the binding energy difference between SO_2 and CO_2 (ΔBE(SO_2/CO_2)) is in the order of –NH– > –C≡C– > –C–C– > –C_3N_3– > –C=C– > –S– (Table 1). As the selective separation of SO_2 over CO_2 depends much on ΔBE(SO_2/CO_2), this linkage screening approach could be a feasible method to effectively construct CMPs for the deep removal of SO_2 from CO_2.

To make the screening results reliable, we synthesized a CMP of TMM–PD with the –NH– linkage through Buchwald–Hartwig amination between tetrakis(4-bromophenyl)methane (TMM) and *p*-phenylenediamine (PD). Meanwhile, TMM–BA containing –C–C– linkage was also constructed through Suzuki–Miyaura cross-coupling by employing the same TMM core but replacing the monomer with 1,4-phenylenebisboronic acid (BA) (Fig. 2a). The successful constructions of TMM–PD and TMM–BA are confirmed by Fourier transform infrared (FT-IR) spectra, with the absence of the characteristic peaks of amino group at 3383 cm^{-1} and 3318 cm^{-1} in the TMM–PD spectrum and the disappearance of the B–O peak at 640 cm^{-1} in the TMM–BA spectrum, respectively (Fig. S5†). Further evidence came from the appearance of the absorption peak of –NH– linkage at 399.7 eV and the C–N bond at 285.2 eV in the X-ray photoelectron spectroscopy (XPS) spectra (Fig. S6†). TMM–PD also has characteristic resonances at ∼62 ppm and ∼150 ppm in solid-state nuclear magnetic resonance (ssNMR) spectra, suggesting the successful Buchwald–Hartwig amination condensation (Fig. S7†). Determined using the N_2 adsorption isotherms at 77 K, the Brunauer–Emmett–Teller (BET) surface areas of TMM–PD and TMM–BA are similar at 526 m^2 g^{-1} and 567.59 m^2 g^{-1}, respectively (Fig. S8a†). However, due to the relatively soft –NH– linkage in TMM–PD in comparison with the rigid C–C linkage between two aromatic benzene rings in TMM–BA, the dominant micropore size in TMM–PD (1.1 nm) is smaller than that in TMM–BA (1.8 nm) and the pore volume of TMM–PD (0.11 cm^3 g^{-1}) is only half of that of TMM–BA (0.22 cm^3 g^{-1}) (Fig. S8b†). The microporosity is further verified by the transmission

Table 1 Summary of BEs of chosen six linkages with SO_2 and CO_2[a]

linkage	–C–C–	–C=C–	–C≡C–	–NH–	–C_3N_3–	–S–
SO_2	11.8	11.5	14.9	−21.4	−13.82	−11.8
CO_2	−5.8	−5.8	−6.6	−7.8	−7.92	−5.8
ΔBE	6	5.7	8.3	13.6	5.9	6

[a] Unit: kJ mol^{-1}.

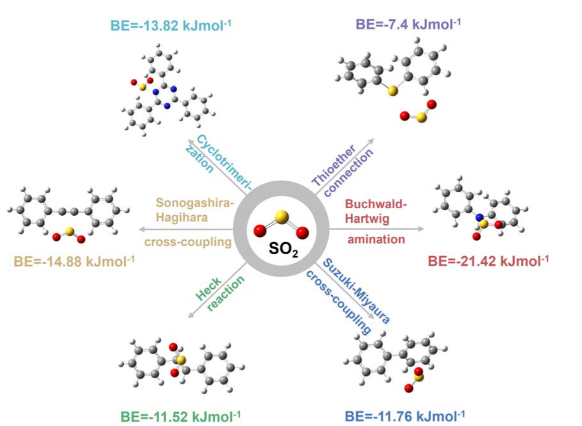

Fig. 1 BEs between a SO_2 molecule and different CMP linkages that were extracted from the typical coupling reactions of Suzuki–Miyaura cross-coupling, Heck reaction, Sonogashira–Hagihara cross-coupling, Buchwald–Hartwig amination, cyclotrimerization, and thioether connection.

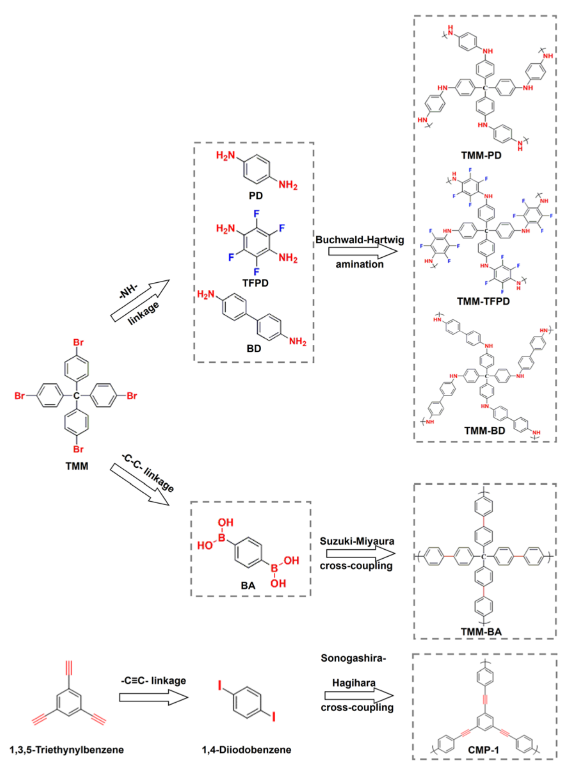

Fig. 2 Schematic synthesis of TMM–PD, TMM–TFPD, TMM–BD, TMM–BA, and CMP-1 through Buchwald–Hartwig amination, Suzuki–Miyaura cross-coupling, and Sonogashira–Hagihara cross-coupling respectively (red color: condensation sites and blue color: functional groups).

electron microscopy (TEM) images, but the morphologies of two-dimensional graphene-like TMM–PD and spherical TMM–BA are quite different (Fig. S9†).

The SO_2 and CO_2 adsorption isotherms provide clear evidence of reversible desulfurization performances of the obtained CMPs. It turns out that at a high pressure of 1 bar, the SO_2 capacities at 273 K of TMM–PD (11.34 mmol g^{-1}) and TMM–BA (10.82 mmol g^{-1}) are similar to each other due to their closed surface area and each shows a decline to 6.65 mmol g^{-1} and 7.54 mmol g^{-1} at 298 K, respectively (Fig. 3a and b). Meanwhile, the CO_2 capacities of TMM–PD (2.6 and 1.7 mmol g^{-1}) and of TMM–BA (2.1 and 1.2 mmol g^{-1}) were much lower at 273 K and 298 K (Fig. S10†), demonstrating the great potential of CMPs for SO_2/CO_2 selective separation. Considering that SO_2 is usually in a trace amount in the flue gas, the adsorption performance at low pressure is lethal for deep desulfurization. Comparing the adsorption performance at a low pressure of 0.1 bar, TMM–PD shows much higher SO_2 capacity (3.2 mmol g^{-1}) than TMM–BA (2.1 mmol g^{-1}) (Fig. 3c), demonstrating the higher SO_2 affinity of –NH– linkage compared to –C–C– linkage. We further used the Grand Canonical Monte Carlo (GCMC) simulation to vividly illustrate the adsorption processes (Fig. S11†). Consistent with the experimental results, both TMM–PD and TMM–BA have much higher SO_2 capacities than CO_2. Moreover, in comparison with TMM–BA, TMM–PD shows higher SO_2 density, and most SO_2 molecules stay around the –NH– linkages, proving that the –NH– linkages in CMPs are beneficial for SO_2/CO_2 separation.

Significantly, based on the ideal adsorbed solution theory (IAST), for the simulated flue gas with 0.2% SO_2, the SO_2/CO_2 selectivity of TMM–PD was calculated to be as high as 113 using the dual site Langmuir–Freundlich model, much higher than 37 in TMM–BA (Fig. 3d). Furthermore, by fitting the SO_2 adsorption isotherms at 273 K and 298 K through the virial-type expression, the adsorption heat (Q_{st}) of SO_2 and CO_2 of TMM–PD and TMM–BA were calculated to be (31.7 *vs.* 13.4 kJ mol^{-1}) and (27.9 *vs.* 29.3 kJ mol^{-1}) at zero coverage, respectively (Fig. S12†). The higher Q_{st} of SO_2 and much lower Q_{st} of CO_2 confirmed that TMM–PD with –NH– linkage has greater potential for selective SO_2 separation than TMM–BA with –C–C– linkage. Besides, this relatively low Q_{st} of 31.7 kJ mol^{-1} also ensures an excellent reversible physical adsorption–desorption performance. By comparison, the excellent SO_2 adsorption capacity of TMM–PD is much higher than that of most reported adsorbents, such as MOFs of MFM-305-CH_3 (5 mmol g^{-1}),[25] SIFSIX-3-Ni (2.74 mmol g^{-1}),[19] Co-gallate (5.2 mmol g^{-1}),[11] organic polymer of P(TMGA-*co*-MBA) (4.06 mmol g^{-1}),[26] traditional porous materials of active carbon (3.3 mmol g^{-1}),[27] and zeolite 13X (2.7 mmol g^{-1} at 323 K and 0.4 bar),[28] and is comparable with that of the benchmark materials SIFSIX-2-Cu-I (6.9 mmol g^{-1}) and NOTT-300 (8.12 mmol g^{-1}).[2,19] Moreover, the SO_2/CO_2 IAST selectivity in TMM–PD is also higher than that of the most reported MOFs, such as the ELM type of ELM-12 (30-13.1),[29] ECUT types of ECUT-111 (25.2-22.2)[14] and ECUT-100 (27.5-26.9),[30] MFM types of MFM-300(In) (33.6-11.6)[31] and MFM-601 (67.5-36.2),[32] and SIFSIX types of SIFSIX-1-Cu (70.7-54.1)[19] and SIFSIX-2-Cu-i (89.4-87.1).[19] The relatively low Q_{st} values are comparable with those of other reported MOF adsorbents such as benchmark adsorbents of Mg-gallate (49 kJ mol^{-1}),[11] SIFSIX-2-Cu (36.1 kJ mol^{-1}),[19] and MFM types of MFM-300(In) (34.5 kJ mol^{-1}),[31] MFM-601 (38 kJ mol^{-1}),[32] and MFM-202a (35 kJ mol^{-1}),[33] suggesting the potential benefit of the temperature swing recycle usage.

To further evaluate the accuracy of the screening results, we synthesized –C≡C– linkage-based CMP-1 through Sonogashira–

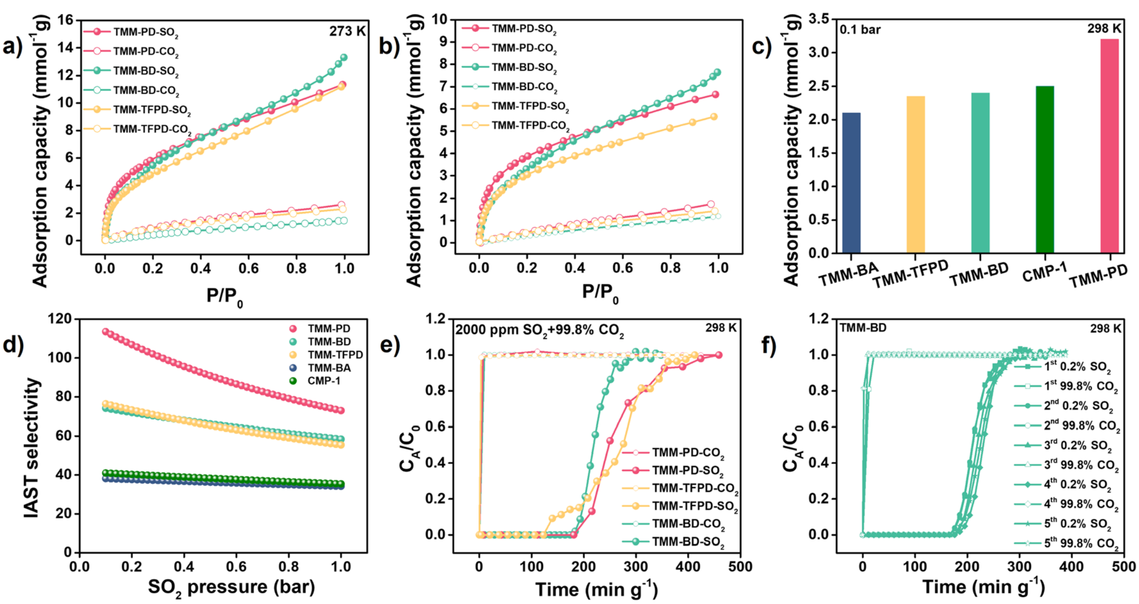

Fig. 3 SO_2 and CO_2 adsorption isotherms of TMM–PD, TMM–TFPD and TMM–BD at (a) 273 K and (b) 298 K. (c) SO_2 adsorption capacity of TMM–PD, TMM–TFPD, TMM–BD, TMM–BA, and CMP-1 at 0.1 bar and 298 K. (d) IAST selectivity of SO_2/CO_2 in TMM–PD, TMM–TFPD, TMM–BD, TMM–BA, and CMP-1 at 298 K. (e) Dynamic breakthrough curves of SO_2 and CO_2 from the mixed gas (2000 ppm SO_2) with a flow rate of 20 mL min^{-1} at 298 K and 1 bar. (f) Cycling dynamic breakthrough curves for CO_2/SO_2 (2000 ppm SO_2) separations in TMM–BD.

Hagihara cross-coupling by reacting 1,4-diiodobenzene with 1,3,5-triethynylbenzene (Fig. 2). Not surprisingly, CMP-1 exhibited favourable SO_2 adsorption uptakes at 1 bar with 14.7 mmol g^{-1} at 273 K and 9.3 mmol g^{-1} at 298 K (Fig. S10†). However, compared with TMM–PD, CMP-1 showed lower SO_2 uptakes at 0.1 bar (2.5 mmol g^{-1} *vs.* 3.2 mmol g^{-1}) and IAST selectivity (41 *vs.* 113) (Fig. 3c and d). Therefore, combining high SO_2 capacity, high SO_2/CO_2 selectivity, and low-energy consumption for regeneration, TMM–PD constructed by –NH– linkage *via* Buchwald–Hartwig amination can be one of the first-class adsorbents for deep desulfurization, further proving the success of our approach for fabricating target-specific CMPs.

As the –NH– linkage *via* Buchwald–Hartwig amination can be achieved using various monomers with specific functional groups, to further demonstrate the feasibility of this novel screening strategy for preparing CMPs with high SO_2/CO_2 separation performance, we developed TMM–BD and TMM–TFPD by replacing PD with benzidine (BD) and 1,3-diamino-2,4,5,6-tetrafluorobenzene (TFPD) to regulate the porosity and hydrophobicity of the CMPs, respectively (Fig. 2a). The successful formation of –NH– linkage in CMPs is demonstrated by the appearance of peaks of the –NH– bond at 399.7 eV and C–N bond at 285.2 eV in the XPS spectra (Fig. S13†). Meanwhile, the new peak of the C–F bond at 687 eV suggests the incorporation of fluorine in TMM–TFPD. Moreover, ssNMR spectra also proved the successful preparation of TMM–BD and TMM–TFPD with the absence of characteristic resonances at ~62 ppm and ~150 ppm (Fig. S7†). With the pore volume doubled (0.22 cm^3 g^{-1}) that of TMM–PD (Fig. S14†), TMM–BD shows a higher SO_2 capacity of 13.3 mmol g^{-1} at 273 K and 1 bar, whereas an almost unchanged SO_2 capacity of about 2.5 mmol g^{-1} at 298 K and low pressure of 0.1 bar further demonstrates the dominant contribution of –NH– linkage to the desulfurization of the flue gas (Fig. 3c). Interestingly, although the BET surface area of TMM–TFPD (254.17 m^2 g^{-1}) decreases to a half less than that of TMM–PD (Fig. S14†), TMM–TFPD still shows an excellent SO_2 capacity of 11.18 mmol g^{-1} at 273 K and 1 bar. It is worth mentioning that the presence of 5–7% water in flue gas would cause a significant decline in desulfurization performance.[34] The hydrophobic modification makes the saturated water uptakes in TMM–TFPD decrease from 10 mmol g^{-1} in TMM–PD to 7 mmol g^{-1} at 298 K (Fig. S15†), suggesting that TMM–TFPD has potential to provide a good microenvironment for the desulfurization of flue gas in the presence of water.

To figure out the mechanisms of this extraordinary SO_2 adsorption and the low porosity but high SO_2 capacity of TMM–TFPD, we recorded the adsorption processes through the *in situ* FTIR spectra (Fig. S19†). During the adsorption of the 2000 ppm SO_2 simulated flue gas, the absorption peaks of TMM–PD and TMM–TFPD changed significantly within 60 min. For TMM–PD, the peak of the –NH– linkage at 1143 cm^{-1} shows a redshift of 4 cm^{-1}, suggesting that it is the active site for SO_2 adsorption (Fig. 4c) whereas the S–O stretching peak at 1347 cm^{-1} in SO_2 shows an obvious red shift of 5 cm^{-1}, ascribed to the electrostatic attraction by the –NH– linkage (Fig. 4c). For TMM–TFPD, the characteristic peaks of –NH– linkage and the S–O bond show a much more complex behavior upon SO_2 adsorption.

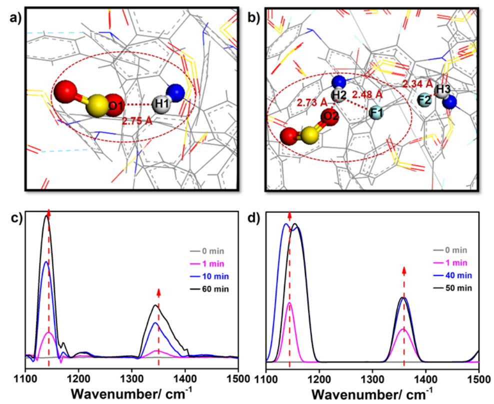

Fig. 4 Visualization of SO_2-binding sites in (a) TMM–PD and (b) TMM–TFPD. *In situ* FTIR spectra of (c) TMM–PD and (d) TMM–TFPD at various times within 60 min under 2000 ppm SO_2 at 298 K.

Specifically, the peaks of –NH– linkage have a blue shift of 2 cm^{-1} during the initial 30 min (Fig. 4d). Subsequently, the peak splits into double ones at 40 min and combines into one peak again during the final 50–60 min (Fig. 4d). We assumed that the small surface area of TMM–TFPD may be attributed to the intramolecular hydrogen bonds between –NH– linkages and fluorine substituents (Fig. S17†) and the adsorption of SO_2 at the –NH– linkage would break hydrogen bonds, further swelling TMM–TFPD for exposing more adsorption sites.[35] This ratiocination is conducive to the complex changes of the –NH– linkage peak where the double splitting can be attributed to the competitive attractions between fluorine and SO_2, and the reunion further demonstrated the strong affinity of –NH– linkage to SO_2. Therefore, the relatively high Q_{st} of SO_2 adsorption of 62 kJ mol^{-1} in TMM–TFPD can be caused by the breakage of hydrogen bonds between –NH– and fluorine. To gain deep insights into this breathing phenomenon, we also performed a GCMC simulation of the SO_2 adsorption in amorphous TMM–PD and TMM–TFPD cells (Fig. S18†). Notably, attributed to the strong electrostatic interaction between $O^{\delta-}$ of SO_2 and $H^{\delta+}$ of –NH– linkage, the distance between SO_2 and –NH– linkage was similar at about 2.75 Å in TMM–PD and TMM–TFPD (Fig. 4), demonstrating that the –NH– linkage is the binding site for SO_2 adsorption, whereas the distance between the –NH– and fluorine bond increased from 2.34 Å to 2.48 Å after SO_2 adsorption in TMM–TFPD, which is consistent with the complex evolution of the –NH– peak in the *in situ* FTIR spectra, further verifying that the adsorption of SO_2 can swell TMM–TFPD through breaking hydrogen bonds of –NH– and fluorine.

The dynamic breakthrough test was further conducted on the simulated flue gas of 2000 ppm SO_2 and 99.8% CO_2 to evaluate the practical implementation of deep desulfurization. At a flow rate of 20 mL min^{-1}, the eluted CO_2 concentration was as high as 99.99% and the elution time of SO_2 was achieved as 180 min g^{-1}, 185 min g^{-1}, and 122 min g^{-1} on TMM–PD, TMM–BD, and TMM–TFPD, respectively (Fig. 3e). Accordingly, the dynamic adsorption capacities were calculated to be 0.47 mmol g^{-1}, 0.4 mmol g^{-1}, and 0.4 mmol g^{-1}, in comparison with their static SO_2 adsorption performance at 0.002 bar (corresponding to a SO_2 content of 2000 ppm) (Fig. 3b). Therefore, under the guidance of the DFT calculations, the CMPs with –NH– linkage produced by Buchwald–Hartwig amination all showed excellent desulfurization performance for trace SO_2 removal, superior to most state-of-the-art materials under similar operating conditions, such as polymers of 70 min g^{-1} in P(3DVB-[VEIm]Br),[22] MOFs of 76 min g^{-1} in MFM-300 (Cr),[36] 152 min g^{-1} in Cage-U-Co-MOF,[37] 180 min g^{-1} in ECUT-111,[30] 60 min g^{-1} in MFM-601,[19] and 28 min g^{-1} in MFM-600,[19] and other traditional zeolites of NaX, FAU, LTA, and SBA-15,[4,5,7,8] demonstrating the successful *de novo* design and screening of taking validated linkages into account for CMP preparation towards the specific deep desulfurization task (Table S2†). Furthermore, flue gas always contains other contaminants such as NO_2 and HCl, which will result in a complicated system for practical separation.[38] Based on our successful strategy, we further calculated the binding efficiency of the –NH– linkage with N_2, HCl, and NO_2 to provide more information about the potential use of CMPs for industrial desulfurization. As shown in Fig. S20,† the BEs between –NH– linkage with N_2, HCl, and NO_2 are lower than that of SO_2 (-4.8 kJ mol^{-1}, -13 kJ mol^{-1}, and -7.2 kJ mol^{-1} *vs.* -21.42 kJ mol^{-1}), suggesting that the –NH– linkage has higher binding selectivity for SO_2 over other contaminants.

Due to that SO_2 is highly corrosive and few leading materials can be stable in the presence of SO_2, we further performed cyclic breakthrough tests to evaluate the reusability of the synthesized CMPs. First, as shown in Fig. S21,† the desorption curves of SO_2 showed a moderate degree of hysteresis because the molecular flexibility would cause open loop hysteresis due to swelling effects. Moreover, the breakthrough performance did not decline in TMM–BD during five cycles for a 0.2% SO_2/99.8% CO_2 mixture (Fig. 3f). Further PXRD patterns and N_2 adsorption proved that TMM–BD can maintain the structure and porosity after SO_2 adsorption, suggesting its excellent stability and reusability for desulfurization (Fig. S22†). Very recently, amine-based porous organic cages (POCs) have been proven to have great potential for SO_2 capture with the sequence of tertiary amine > second amine > imine.[9] In this system, Liu and co-authors indicated the importance of the basicity of the amine in SO_2 capture. Even though the second amine has a high SO_2 binding efficiency, the strong acid and corrosive nature of SO_2 would destroy the POC structure after removal of the adsorbed SO_2. While for CMPs that were synthesized by Buchwald–Hartwig amination, the electron density of the second amine was decoupled by two connected benzene rings, leading to the retention of the structure and porosity after SO_2 treatment. Moreover, once the optimal linkage to fabricate CMPs for SO_2 capture was identified, the high diversity of the starting monomers could benefit different properties in CMPs such as hydrophobicity, larger pore volume, and pore structure.

Conclusions

In summary, we developed a feasible approach by screening linkages extracted from the coupling reactions for CMPs' construction through calculating the affinity with SO_2 and simulating the SO_2 adsorption density. Under the guidance of the screening results, TMM–PD, TMM–TFPD, and TMM–BD were fabricated *via* Buchwald–Hartwig amination with different porosities and hydrophobicities which showed higher selective SO_2 adsorption performance. In particular, the excellent dynamic SO_2 removal performance of TMM–BD with an elution time of 185 min g^{-1} and a high CO_2 purity of greater than 99.99% was achieved from the simulated flue gas containing 2000 ppm SO_2, superior to the most reported state-of-the-art adsorbents. Moreover, the fluorine functionalized TMM–TFPD significantly increased the water resistance and maintained high SO_2 capacity, providing a potential application for the practical flue gas desulfurization process. Through successfully bypassing the invalid synthesis of screened CMPs from billions of monomers, our work demonstrates the significance of linkage diversities on the intrinsic properties of porous materials and solves the dilemma between the implementability of computational screening and the synthesis of porous materials.

Data availability

Should any raw data files be needed they are available from the corresponding author upon reasonable request.

Author contributions

He Li, Xili Cui, Jun Hu, and Honglai Liu conceived and designed the project. He Li synthesized the materials and carried out all the characterization studies and computational simulations. Hanqian Pan and Yijian Li performed the breakthrough test. All authors participated in data analysis, discussion of the results and manuscript revision.

Conflicts of interest

There are no conflicts to declare.

Acknowledgements

The authors are grateful for the financial support from the National Natural Science Foundation of China (No. 21878076 and 22278126), the Fundamental Research Funds for the Central Universites (2022ZFJH004), and Intergovernmental International Science and Technology Innovation Cooperation Key Project (2021YFE0112800).

Notes and references

1 E. Croiset and K. Thambimuthu, *Fuel*, 2001, **80**, 2117–2121.
2 S. Yang, J. Sun, A. J. Ramirez-Cuesta, S. K. Callear, W. I. David, D. P. Anderson, R. Newby, A. J. Blake, J. E. Parker, C. C. Tang and M. Schroder, *Nat. Chem.*, 2012, **4**, 887–894.
3 H. Yi, H. Deng, X. Tang, Q. Yu, X. Zhou and H. Liu, *J. Hazard. Mater.*, 2012, **203–204**, 111–117.
4 X. Zhou, H. Yi, X. Tang, H. Deng and H. Liu, *Chem. Eng. J.*, 2012, **200–202**, 399–404.

5 A. Czyżewski, J. Kapica, D. Moszyński, R. Pietrzak and J. Przepiórski, *Chem. Eng. J.*, 2013, **226**, 348–356.
6 D. Yang, M. Hou, H. Ning, J. Ma, X. Kang, J. Zhang and B. Han, *ChemSusChem*, 2013, **6**, 1191–1195.
7 H. Deng, H. Yi, X. Tang, H. Liu and X. Zhou, *Ind. Eng. Chem. Res.*, 2013, **52**, 6778–6784.
8 L. Wei, Z. Gao and Y. Wang, *Asia-Pac. J. Chem. Eng.*, 2017, **12**, 660–670.
9 I. Ibarra, E. Martínez-Ahumada, D. He, V. Berryman, V. Jancik, V. Martis, M. A. Vera, E. Lima, D. J. Parker and A. I. Cooper, *Angew. Chem., Int. Ed.*, 2021, **60**, 17556–17563.
10 X. Suo, Y. Yu, S. Qian, L. Zhou, X. Cui and H. Xing, *Angew. Chem.*, 2021, **133**, 7062–7067.
11 F. Chen, D. Lai, L. Guo, J. Wang, P. Zhang, K. Wu, Z. Zhang, Q. Yang, Y. Yang, B. Chen, Q. Ren and Z. Bao, *J. Am. Chem. Soc.*, 2021, **143**, 9040–9047.
12 E. Martinez-Ahumada, M. L. Diaz-Ramirez, M. J. Velasquez-Hernandez, V. Jancik and I. A. Ibarra, *Chem. Sci.*, 2021, **12**, 6772–6799.
13 S. Xing, J. Liang, P. Brandt, F. Schafer, A. Nuhnen, T. Heinen, I. Boldog, J. Mollmer, M. Lange, O. Weingart and C. Janiak, *Angew. Chem.*, 2021, **60**, 17998–18005.
14 M. J. Yin, X. H. Xiong, X. F. Feng, W. Y. Xu, R. Krishna and F. Luo, *Inorg. Chem.*, 2021, **60**, 3447–3451.
15 G. L. Smith, J. E. Eyley, X. Han, X. Zhang, J. Li, N. M. Jacques, H. G. W. Godfrey, S. P. Argent, L. J. McCormick McPherson, S. J. Teat, Y. Cheng, M. D. Frogley, G. Cinque, S. J. Day, C. C. Tang, T. L. Easun, S. Rudic, A. J. Ramirez-Cuesta, S. Yang and M. Schroder, *Nat. Mater.*, 2019, **18**, 1358–1365.
16 K. Tan, S. Zuluaga, H. Wang, P. Canepa, K. Soliman, J. Cure, J. Li, T. Thonhauser and Y. J. Chabal, *Chem. Mater.*, 2017, **29**, 4227–4235.
17 J. Yu, Y. Ma and P. B. Balbuena, *Langmuir*, 2012, **28**, 8064–8071.
18 V. Chernikova, O. Yassine, O. Shekhah, M. Eddaoudi and K. N. Salama, *J. Mater. Chem. A*, 2018, **6**, 5550–5554.
19 X. Cui, Q. Yang, L. Yang, R. Krishna, Z. Zhang, Z. Bao, H. Wu, Q. Ren, W. Zhou, B. Chen and H. Xing, *Adv. Mater.*, 2017, **29**, 1606929.
20 M. R. Tchalala, P. M. Bhatt, K. N. Chappanda, S. R. Tavares, K. Adil, Y. Belmabkhout, A. Shkurenko, A. Cadiau, N. Heymans, G. De Weireld, G. Maurin, K. N. Salama and M. Eddaoudi, *Nat. Commun.*, 2019, **10**, 1328.
21 P. Brandt, A. Nuhnen, S. Öztürk, G. Kurt, J. Liang and C. Janiak, *Adv. Sustainable Syst.*, 2021, **5**, 2000285.
22 L. Xia, Q. Cui, X. Suo, Y. Li, X. Cui, Q. Yang, J. Xu, Y. Yang and H. Xing, *Adv. Funct. Mater.*, 2018, **28**, 1704292.
23 J.-S. M. Lee and A. I. Cooper, *Chem. Rev.*, 2020, **120**, 2171–2214.
24 S. Jiang, K. E. Jelfs, D. Holden, T. Hasell, S. Y. Chong, M. Haranczyk, A. Trewin and A. I. Cooper, *J. Am. Chem. Soc.*, 2013, **135**, 17818–17830.
25 L. Li, I. da Silva, D. I. Kolokolov, X. Han, J. Li, G. Smith, Y. Cheng, L. L. Daemen, C. G. Morris, H. G. W. Godfrey, N. M. Jacques, X. Zhang, P. Manuel, M. D. Frogley, C. A. Murray, A. J. Ramirez-Cuesta, G. Cinque, C. C. Tang, A. G. Stepanov, S. Yang and M. Schroder, *Chem. Sci.*, 2019, **10**, 1472–1482.
26 L. Wu, D. An, J. Dong, Z. Zhang, B.-G. Li and S. Zhu, *Macromol. Rapid Commun.*, 2006, **27**, 1949–1954.
27 Y. Guo, Y. Li, T. Zhu and M. Ye, *Fuel*, 2015, **143**, 536–542.
28 H. Deng, H. Yi, X. Tang, Q. Yu, P. Ning and L. Yang, *Chem. Eng. J.*, 2012, **188**, 77–85.
29 Y. Zhang, P. Zhang, W. Yu, J. Zhang, J. Huang, J. Wang, M. Xu, Q. Deng, Z. Zeng and S. Deng, *ACS Appl. Mater. Interfaces*, 2019, **11**, 10680–10688.
30 L. J. Guo, X. F. Feng, Z. Gao, R. Krishna and F. Luo, *Inorg. Chem.*, 2021, **60**, 1310–1314.
31 M. Savage, Y. Cheng, T. L. Easun, J. E. Eyley, S. P. Argent, M. R. Warren, W. Lewis, C. Murray, C. C. Tang, M. D. Frogley, G. Cinque, J. Sun, S. Rudic, R. T. Murden, M. J. Benham, A. N. Fitch, A. J. Blake, A. J. Ramirez-Cuesta, S. Yang and M. Schroder, *Adv. Mater.*, 2016, **28**, 8705–8711.
32 J. H. Carter, X. Han, F. Y. Moreau, I. da Silva, A. Nevin, H. G. W. Godfrey, C. C. Tang, S. Yang and M. Schroder, *J. Am. Chem. Soc.*, 2018, **140**, 15564–15567.
33 S. Yang, L. Liu, J. Sun, K. M. Thomas, A. J. Davies, M. W. George, A. J. Blake, A. H. Hill, A. N. Fitch, C. C. Tang and M. Schroder, *J. Am. Chem. Soc.*, 2013, **135**, 4954–4957.
34 D. Wang, A. Bao, W. Kunc and W. Liss, *Appl. Energy*, 2012, **91**, 341–348.
35 T. Steiner, *Angew. Chem., Int. Ed.*, 2002, **41**, 48–76.
36 L. Briggs, R. Newby, X. Han, C. G. Morris, M. Savage, C. P. Krap, T. L. Easun, M. D. Frogley, G. Cinque, C. A. Murray, C. C. Tang, J. Sun, S. Yang and M. Schröder, *J. Mater. Chem. A*, 2021, **9**, 7190–7197.
37 Y. Fan, M. Yin, R. Krishna, X. Feng and F. Luo, *J. Mater. Chem. A*, 2021, **9**, 4075–4081.
38 P. N. Chisholm and G. T. Rochelle, *Ind. Eng. Chem. Res.*, 2000, **39**, 1048–1060.